The sensitivity limit of nanoparticle biosensors in the discrimination of single-nucleotide polymorphism

María Sanromán-Iglesias,[a,b] Charles Lawrie,[b,d] Thomas Schäfer,[c,d] Marek Grzelczak,[a,d,e,*] Luis M. Liz-Marzán[a,d,e]

[a] CIC biomaGUNE, Paseo de Miramón 182, 20009 Donostia-San Sebastián, Spain

[b] Oncology Area, Biodonostia Research Institute, Donostia-San Sebastián, Spain

[c] Polymat, University of the Basque Country, Donostia-San Sebastián; and Ikerbasque, Bilbao, Spain.

[d] Ikerbasque, Basque Foundation for Science, 48013 Bilbao, Spain

[e] CIBER de Bioingeniería, Biomateriales y Nanomedicina, CIBER-BBN, 20009 Donostia-San Sebastián, Spain

KEYWORDS nanoparticle, size, single-nucleotide polymorphism, colorimetric detection

ABSTRACT: Detection of single nucleotide polymorphisms (SNP) by selective aggregation of nanoparticles offers a rapid determination of cancer biomarkers, detectable by the naked eye. The main factor limiting the sensitivity of such colloidal sensors is the number of available target DNA molecules that can induce aggregation and thereby transduce an optical output signal. Although particle size is an obvious parameter of choice toward the modulation of the target-to-particle ratio at constant metal concentration, it is often omitted due to difficulties in the synthesis of particles with suitable size or to the limited colloidal stability of large particles stabilized with DNA. We present here a systematic study of SNP detection using gold nanoparticles of various sizes (13, 46 and 63 nm), using a conventional sandwich assay. We found that a five-fold increase in particle size, at constant gold concentration, leads to an improvement in the limit of detection by three orders of magnitude, which is 5, 0.1, and 0.05 nM for 13, 46 and 63 nm, respectively. This assay allows the SNP detection down to 10.85 fmol within less than 10 minutes. We conclude that a target-to-particle ratio equal to 4 sets the limit of detection and sensitivity of the assay, regardless of particle size.

Single nucleotide variations in a DNA sequence, or single-nucleotide polymorphism (SNP), can occur as a result of inheritance, in which case it may be linked to the susceptibility of a given person to a particular disease. Alternatively, SNPs may arise within (somatic) cell populations due to mutation of the DNA sequence. When these variations cause changes in the function of the resulting protein this can be associated with many diseases including cardiovascular or neurodegenerative diseases, and in particular cancer.[1–6] Therefore, the ability to specifically detect SNPs has a significant value in diagnosis, prognosis and prediction of the patient's response to a certain treatment.

A number of techniques have been proposed for SNP discrimination, including high resolution DNA melting analysis,[7–9] single molecule fluorescence,[10] molecular beacons,[11] hybridization chain reactions,[12] surface enhanced Raman scattering,[13] mass spectrometry,[14] electrochemical detection,[15] and DNA hybridization.[16] These methods have however relatively low SNP discrimination ratios (DR < 20×) and/or limited sensitivity.[17]

Over two decades ago, Mirkin's group demonstrated the feasibility of using plasmonic nanoparticles for SNP detection.[18,19] They used a sandwich approach in which gold nanoparticles (AuNPs) capped with different DNA strands underwent aggregation in the presence of a mutually complementary DNA sequence. Interestingly, by introducing a single-base mutation into the analyte sequence, the aggregation was less pronounced. Since then, progress in the field has allowed an increasing complexity in colorimetric assays, thus improving their performance in parameters such as sensitivity, selectivity and detection time.[20–22] In most of these studies, 13 nm gold nanoparticle signal transducers were used, primarily due to the simplicity of the Turkevich synthesis method.[23] Although these nanoparticles are useful for conceptual definition of the assay, their extinction coefficient is low compared to particles with larger diameter ($\sigma_{ext} \propto D^6$),[24] rendering limited capacity of transducing a chemical event into an optical signal. We therefore hypothesized that by using larger NPs the sensitivity of the system could be improved, as at the same concentration of metal, the number of target molecules necessary to observe the aggregation would be lower. In addition, the

lower curvature of larger particles would facilitate multiple binding events by DNA to connect NP probes.[25] We therefore suggest that the main intrinsic limitation of a colloidal biosensor is the ratio of target DNA molecules to nanoparticles.

In this work, we identified the limiting concentration of target DNA molecules needed to induce optical changes in a colloidal solution, as a function of particle size. We used a sandwich type colorimetric assay to detect a SNP in the BRCA1 gene, an important indicator of increased risk to the development of breast and ovarian cancer.[26–28] We demonstrated that a target-to-particles ratio of ~4 was sufficient to discriminate the presence of the single-base mutation. With a five-fold increase in the diameter, the number of particles was lowered by two orders of magnitude, allowing for SNP detection down to 10.85 fmol within less than 10 minutes.

Methods

Chemicals

Hydrogen tetrachloroaurate (III) hydrate ($HAuCl_4 \cdot 3H_2O$) was purchased from Alfa Aesar. Sodium dodecyl sulphate (SDS) (98%), sodium chloride (NaCl) (99.5%), sodium citrate tribasic dihydrate (98%), phosphate buffer solution (PB) 1M, pH 7.4, were purchased from Sigma Aldrich. Phosphate buffered saline (PBS) 0.01 M, pH 7.4, containing 0.138 M NaCl and 2.7 mM KCl (Sigma-Aldrich) was used to mimic physiological conditions. DNA-targets (match and mismatch) and thiolated-oligonucleotides (Figure 1) were purchased from Biomers (Germany).

Figure 1. Scheme displaying the sequences of thiolated oligonucleotides and target DNA (match and mismatch), together with particles of different sizes.

Instrumentation

UV–Visible (UV–Vis) spectra were measured at room temperature on an Agilent 8453 UV-Vis spectrophotometer, using quartz cuvettes with 1.0 cm optical path length. Transmission electron microscopy (TEM) was measured in a JEOL JEM-1400 PLUS, operating at 120 kV, equipped with a GATAN US1000 CCD camera(2kx2k). Dynamic light scattering (DLS) measurements were carried out in a Malvern NanoSizer.

Synthesis of Au nanoparticles

13 nm AuNPs were prepared according to the standard Turkevich method.[23] In brief, a solution of $HAuCl_4$ (500 mL, 0.5 mM) was heated up to boiling in an 1 L Erlenmeyer flask, followed by the addition of trisodium citrate solution (25 mL, 1% w/v) under vigorous stirring. After 15 min of boiling, the solution was set aside to cool down to room temperature and stored at 4 ºC for further use. The final concentration of metallic gold was 0.5 mM.

46 nm and 63 nm AuNPs were synthesized following an Au-assisted seeded growth method.[29] *Synthesis of Au seeds*: a solution of trisodium citrate (150 mL, 2.2 mM) was heated for 15 min under vigorous stirring until boiling, followed by injection of a solution of $HAuCl_4$ (1 mL, 25 mM). The color of the solution changed from yellow to blueish gray and then to light pink in 10 min. *Seeded Growth*: The seeded growth process comprised cyclic addition of metal precursor and extraction of particles product. In a typical process, the seed solution was cooled down to 90 °C and then $HAuCl_4$ solution (1 mL, 25 mM) was added, followed by a second addition after 30 minutes. After a further 30 min period, part of the growth solution (55 mL) was extracted and to the remaining solution (98 mL) water (53 mL) and sodium citrate (2 mL, 60 mM) were added. This addition/extraction process was repeated 3 times to obtain gold nanoparticles with 46 nm in diameter (55 mL). Further repetition of the process yielded 63 nm AuNPs (55 mL). The final concentration of metallic gold was 0.8 mM in both samples.

Functionalization of AuNPs

AuNPs were functionalized with thiolated oligonucleotides (1Triplex and 2Triplex) according to the method reported by Hurst *et al.*[30] Briefly, to the AuNPs colloid (1.25 mL) containing SDS (0.1 %) and PBS (0.01 M) was added a solution of oligonucleotides to reach a final concentration of 1 OD/mL. We used in all samples excess oligonucleotides, estimated as 2, 3 and 4 oligonucleotides per nm^2 of gold surface, for 13, 43 and 63 nm AuNPs, respectively. The mixture of oligonucleotides and AuNPs was incubated at room temperature for 20 min. To improve oligonucleotide binding onto the gold surface, a salt aging process was carried out. A solution containing NaCl (2 M), SDS (0.01 %) and PBS (0.01 M) was added sequentially to the mixture containing AuNPs and oligonucleotides in the following aliquots: 5, 5, 15, 25 and 50 µL, ultimately reaching a final NaCl concentration of 0.2 M. After each addition the mixture was sonicated for 10 s followed by a 20 min incubation period. The final solution was incubated for 12 hours. To remove excess oligonucleotides, the solutions were centrifuged three times (13 nm at 13000 rpm for 20 min; 46 nm at 8500 rpm for 15 min; 63 nm at 8500 rpm for 10 min), each time redispersed in SDS (1 mL, 0.01 %). The final concentration of nanoparticles was 0.4 mM in terms of metallic gold for all samples.

Hybridization of AuNP-DNA probes and detection of ssDNA targets

Equal volumes (62.5 µL) of two batches containing Au@DNA (Au@1Triplex and Au@2Triplex) were combined into the cuvette, followed by the addition of PBS (x 1, 325 µL). To this solution was added 50 µL of a mixture containing PB (0.01 M) and NaCl (2 M) to reach the final volume of 0.5 mL. Finally, an aliquot of target ssDNA (either match or mismatch of desired concentration) was added to the solution. Immediately after the addition of target ssDNA, UV-Vis spectra were recorded during 30 min at 0.5 min intervals. Since the stock solutions containing Au@DNA ([Auo]=0.4mM) were stored in 0.01% SDS (vide supra), the final concentration of the surfactant was 0.001% while the final concentration of metallic gold was 0.01 mM. The pH of the mixture was 7.4. The final concentration of NaCl was 0.33 M, which was the optimal concentration to balance fast response of the assay (~10 min) and greatest selectivity toward single based mutation (Figure S1).

Results and discussion

It is well known that gold nanoparticles stabilized with sodium citrate can be readily functionalized with other thiolated ligands. We initially synthesized AuNPs with an average diameter of 13.3 ± 1.2 nm, using the traditional Turkevich method,[31] and these particles were used as seeds to grow larger AuNPs (45.9 ± 5.8 and 62.4 ± 6.5 nm in diameter), as described by Bastús *et al.*[29] (for simplicity, we label the corresponding AuNPs as 13, 46 and 63 nm). All AuNPs displayed relatively low polydispersity values of 9%, 13% and 11%, for 13 nm, 46 nm and 63 nm, respectively (Figure 2a-c). The replacement of citrate by the corresponding ssDNA was carried out as described by Mirkin's group,[30] by mixing AuNPs of different sizes with excess of thiol-terminated oligonucleotides (1 OD/mL). To maximize surface coverage of the particles with oligonucleotides the salting out process was applied using 0. 2 M NaCl. The results reported in ref. 30 allow estimation of a number of DNA per particle: 80 DNA/NP for 13 nm, 450 DNA/NP for 46 nm, and 750 DNA/NP for 63 nm nanoparticles.

The maxima of the localized surface plasmon resonance (LSPR) bands of AuNP colloids were 519 nm, 535 nm and 538 nm, for 13, 46 and 63 nm AuNPs, respectively. The presence of ssDNA on the particles surface caused a slight LSPR redshift of 2-5 nm, regardless of the particle size (Figure 2d), due to the increase in local refractive index. The presence of ssDNA on the particles surface was confirmed by DLS measurements before and after functionalization. As expected, the hydrodynamic diameters increased by ~10 nm (Figure 2e). In the case of 46 nm AuNPs, however, the increase of the recorded hydrodynamic diameter was less pronounced, likely due to a higher polydispersity (13%) of the sample.

To evaluate the effect of particle size on the discrimination of single-nucleotide polymorphism we choose BRCA1 gene, which is one of the most studied genes in the context of the single-based mutation. To ensure relatively facile discrimination of the mutation we parameterized the match and the mismatch sequences according to the nearest-neighbor model,[32] which dictates following structural requirements: (1) central position of the mutation in the sequence; (2) relatively short sequences (19 bases); (3) low CG content (26% for mismatch and 31% of match); (4) mismatch type affecting C–G base pair instead of A-T. (see Figure 1).

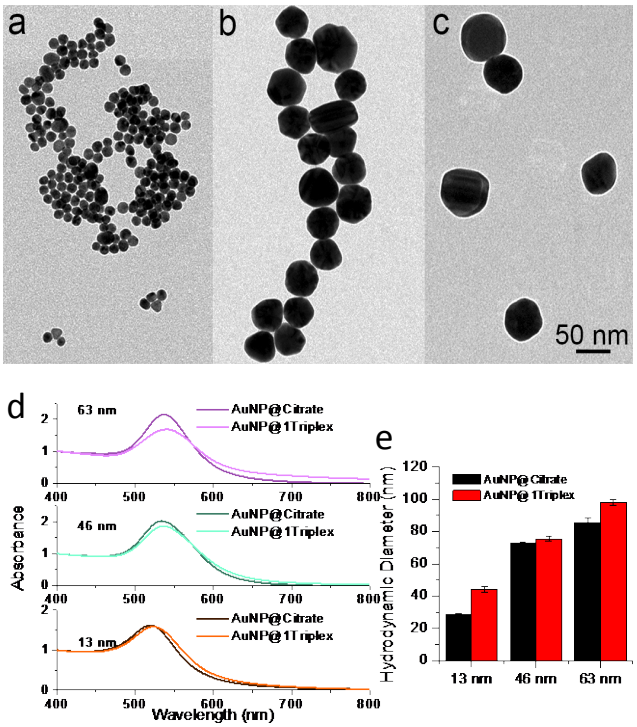

Figure 2. Gold nanoparticles used in this study. (a-c) TEM images of initial AuNPs with different diameters: 13 nm (a), 46 nm (b) and 63 nm (c). (d) UV-Vis spectra of AuNPs stabilized with citrate and DNA (2Triplex). (e) Average hydrodynamic diameters of initial, citrate-stabilized AuNPs (black bars) and AuNP-1Triplex (red bars).

To discriminate the mutation we used a sandwich assay[33] involving the addition of a target sequence (either match or mismatch) to the mixture of probe nanoparticles, AuNP-1Triplex and AuNP-2Triplex. The bridging of probe nanoparticles by the complementary target was expected to promote aggregation of the nanoparticles, in turn affecting the optical properties of the colloid.[34,35] In particular, the LSPR bands are expected to redshift and broaden, as a result of aggregation and plasmon coupling (see Supplementary Information, Figure S2). The aggregation of the particles was monitored over time by UV-Vis spectroscopy, using the unitless magnitude $R = Abs_{620}/Abs_{max}$, as a measure for the degree of aggregation.[36] Before target addition, the value R_o ranged in our assay between 0.2 and 0.4. Once the target was added to the probes solution, R increased

to reach a maximum value of ~1.2 (best scenario). In addition, upon aggregation, the characteristic absorption band for oligonucleotides, located at 260 nm, was found to gradually decrease (Figure S2), due to delocalization of the excitonic states in denatured DNA.[37]

To properly evaluate the sensitivity of the assay for different particle sizes, the concentration [Au^0] = 0.1 mM was kept constant in all experiments. Therefore, changes in particle diameter affected the number of particles (expressed in molar concentration) for each assay. The concentration of particles was: 1.5 nM, 0.033 nM and 0.013 nM, for 13, 46 and 63 nm, respectively. Note that, adjusting the assays to a constant number of particles (as opposite to Au^0 concentration) was unpractical due to the dramatic difference in extinction cross section for different particle sizes. For example, bringing the concentration of 13 nm AuNPs down to 0.013 nM made it impossible to record a meaningful UV-Vis spectrum (Figure S3). In addition, the difference in absorbance affected the value of R_0, which hindered a comparative analysis (Figure S4).

Each probe solution containing particles of different sizes was incubated with both the match and mismatch target sequences, in the range between 50 and 0.05 nM (Figure 3). As expected, with increasing particle size, the sensitivity of the assay also increased. The smaller AuNPs (13 nm) aggregated in the presence of match sequence, within a concentration range between 50 and 5 nM. For the mismatch sequence however, aggregation was only observed for concentrations above 50 nM. The intermediate AuNPs (46 nm) aggregated in the presence of the match sequence at a broader concentration range between 50 nM and 0.25 nM. For the mismatch sequence, aggregation was detected for target concentrations above 5 nM. Finally, the larger particles (63 nm) were sensitive to an even wider concentration range (50 nM to 0.05 nM) of the match sequence, but only between 5 and 50 nM for the mismatch sequence. These results clearly suggest that the sensitivity of the assay depends on the available number of target molecules per particle. A careful comparison of the concentrations of target and particles revealed that it was necessary to add ~ 4 molecules of match sequence per particle to induce meaningful changes in the R value. (For a complete list of target-to-particle ratios see Supporting Information Table S1). Interestingly, the concentration of the mismatch sequence that was required to induce aggregation was 20-40 times higher than the concentration of nanoparticles, showing that the single-base mutation has a large impact on the aggregation process.

To further evaluate the aggregation process, we measured the time-dependent growth of the aggregates, using DLS. We used a fixed concentration (5 nM) of match and mismatch sequences, yielding the following target-to-particle ratios: ~3 (13 nm), ~150 (46 nm) and ~380 (63 nm). We hypothesized that the small nanoparticles should remain stable, since not sufficient target was provided, while the bigger particles should aggregate. As shown in Figure 4a-b, when exposed to the match sequence, the aggregates containing NPs of 46 nm and 63 nm were 2.5-fold larger than those from the same particles after one hour in the presence of the mismatch sequence. After 60 minutes of aggregation in the presence of the match sequence, the clusters were *ca.* 550 nm in diameter for both 46 and 63 nm AuNPs, corresponding to ~150 and ~320 particles per cluster, respectively. In the case of small NPs, no aggregation was observed when the mismatch sequence was used (Figure 4c). In the presence of the match sequence, the measured diameter increased up to 20 nm, which is likely related to intercalation of target DNA with the complementary DNA attached to the particle surface. No further aggregation was observed upon extended incubation, probably due to an insufficient number of target molecules per particle (~3).

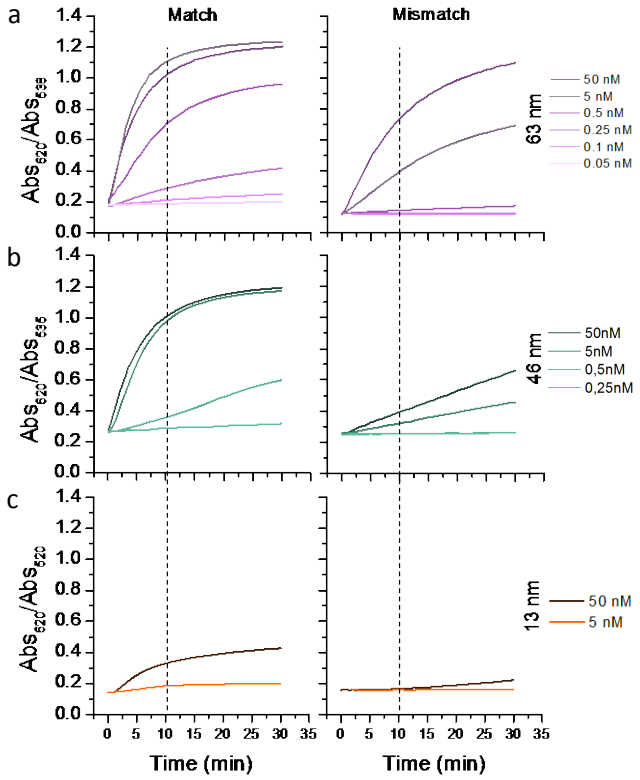

Figure 3. Sensitivity of the assay for AuNPs with different diameters. Comparison of the aggregation degree for match (left column) and mismatch (right column) sequences, with AuNPs of different sizes: a) 63 nm, b) 46 nm, c) 13 nm. [Au^0] = 0.1 mM for all cases, while [AuNPs] varied as: 1.5, 0.033, 0.013 nM, for 13, 46 and 63 nm, respectively.

TEM analysis of the aggregates (in the presence of the match sequence) was performed at 1, 10 and 15 minutes after target addition (Figure 4d-f). The number of particles per aggregate increased from 3-5 to 15-20 for 1 and 10 minutes, respectively. After 15 minutes, the diameter of the aggregates was nearly 1 µm, i.e. >100 AuNPs. Note that the diameter of the aggregates on TEM grids appears larger than in solution due to flattening upon drying.

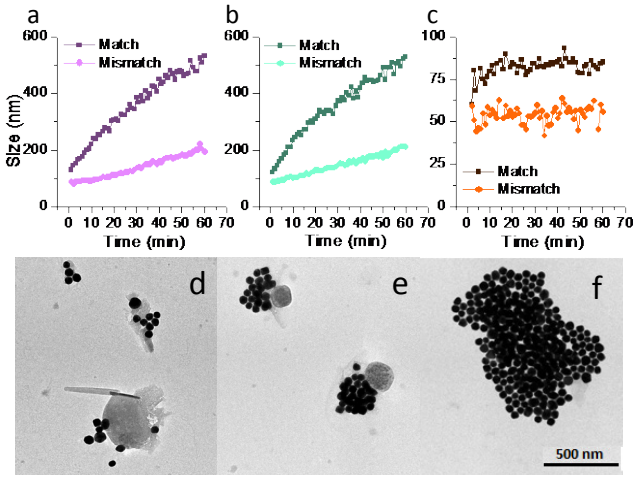

Figure 4. a-c) DLS measurements for the hybridization process using the match and mismatch sequences at 5 nM concentration for AuNPs of a) 63 nm, b) 46 nm and c) 13 nm. **d-f)** TEM images of aggregates formed upon hybridization with the match sequence at a concentration of 5 nM for AuNP of 63 nm at d) 1 min, e) 10 min and f) 15 min.

Several control experiments were additionally conducted. No aggregation was observed in the absence of the target ssDNA for 63 nm AuNPs (Figure S5). A melting profile analysis confirmed the selective role of the match sequences in the particle aggregation. For the match sequence, a sharp transition in the profile was observed at 43 °C, whereas for the mismatch sequence no change in particle size was detected (Figure S6). The heating process had no effect on the stability of the particles, as cyclic aggregation kinetics showed a similar degree of aggregation during three cycles of heating (Figure S7).

We next evaluated the effect of particle size on the selectivity of the assay. We compared the values of R for the match and mismatch after 10 min of aggregation (see vertical dashed line in Figure 3). The values of R for selected particle sizes and target concentrations are shown in Figure 5a, demonstrating that the values of R converge for match and mismatch sequences when decreasing the concentration of the target. Further analysis of the selectivity allowed us to differentiate the value of R_{match} from $R_{mismatch}$ after 10 minutes of aggregation (Figure 5b). We can see that a target concentration window can be identified for the bigger particles, at which they display the best sensing performance, for example we can differentiate between the match and mismatch down to 0.05 nM using the 63 nm particles. However, with increasing target concentration the difference becomes less pronounced. This behavior is due to a cooperative effect, meaning that the lower curvature of the larger particles facilitates aggregation through binding more than one DNA target molecule per particle. Note that at 50 nM target concentration, each 63 nm particle carries ~4000 target molecules for either match or mismatch DNA. Therefore, the differentiation between match and mismatch is less pronounced if multiple binding events take place.[33] When decreasing the particle size to 46 nm, the selectivity between the match and mismatch at higher concentration (50 nM) is better than that for 63 nm particles (Figure 5b). We assume that the higher curvature in 46 nm particles minimizes the cooperative effect and favors the specificity of the system at higher target concentrations. However, at lower target concentrations (< 1 nM) the system becomes less specific due to the smaller number of available DNA target molecules per particle. Accordingly, for the small (13 nm) particles the specificity increases with increasing target concentration, but with no selectivity below 5 nM.

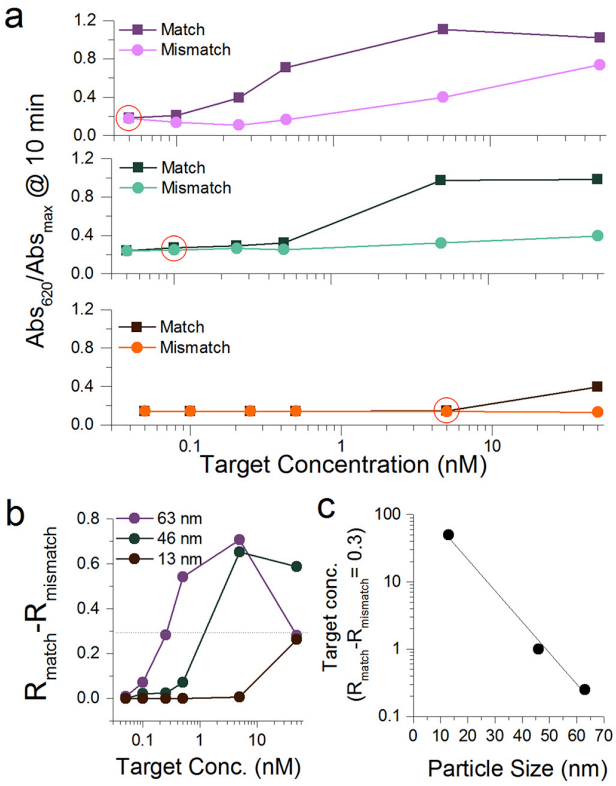

Figure 5. Selectivity between match and mismatch sequences for different concentrations of target, using AuNPs of different sizes. a) Differences in the aggregation degree (Abs_{620}/Abs_{max}) for the different particle sizes, at a target concentration range from 50 to 0.05 nM. The points circled in red represent limit of selectivity (match/mismatch) and corresponds to target-to-particle ratio equal to 4. b) Difference between R values for match and mismatch versus target concentration, showing better specificity for larger particles. c) Target concentration at R_{match}-$R_{mismatch}$ = 0.3 versus particle size, showing a linear dependence in a logarithmic scale.

To further show how the particles dimension affects the performance of the assay we correlated the selectivity of the assay at constant specificity with particle diameter. A plot of target concentration at R_{match}-$R_{mismatch}$ = 0.3 (dotted line in Figure 5b) versus particle diameter shows a linear dependence in a semi-log plot (Figure 5c). This relationship indicates that a 5-fold increase in particle

size leads to an improvement of SNP differentiation by 3 orders of magnitude. In other words, by using as few as 150 nm particles, we should be able to differentiate SNP down to 10 fM. These results show that the design of the colloidal assay for biomolecule detection requires a precise knowledge of the concentration window for the target to be detected.

As mentioned above, the target-to-particles ratio is an important parameter defining the limits of the colloidal assay. For the 63 nm AuNPs, for example, we showed that a ratio of 4 is the minimum required to appreciate aggregation, which corresponds to 50 pM of match DNA (Figure 5 and Figure 6a). We thus propose that a further decrease of particle and target concentrations (keeping the target-to-particle ratio constant ~4) the limit of detection can be improved further. We thus show in Figure 6b the time evolution of R using 10 pM of match and mismatch DNA with an AuNP concentration of 3 pM. A meaningful difference between match and mismatch is observed after 10 min of aggregation. However, when decreasing the target concentration down to 5 pM while keeping the target-to-particle ratio = 4, a significant fluctuation of the R-value was observed for both match and mismatch (Figure 6c). These results confirm that the limits in colorimetric assays are related to the minimum number of target molecules available to induce particle aggregation, clearly indicating that the target concentration should always be larger than that of nanoparticles. We additionally carried out an experiment using a target-to-particle ratio of 0.8 (13 nM NPs and 10 nM of target), which confirmed the lack of differentiation between match and mismatch, 10 minutes after target addition (Figure S8).

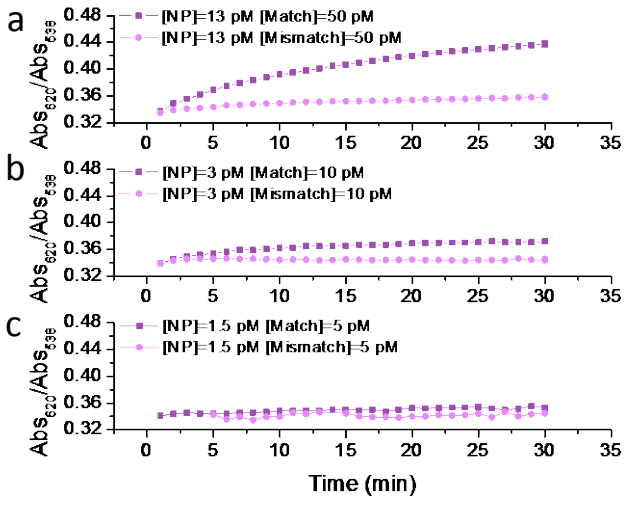

Figure 6. Comparison of the degree of aggregation during the detection of the match sequence at different concentrations: a) 50 pM, b) 10 pM and c) 5 pM, using [AuNPs]: 13 pM, 3 pM and 1.5 pM, respectively.

Conclusions

We analyzed the effects of nanoparticle size on the sensitivity and selectivity of a colorimetric detection assay of the BRCA1 mutation. We demonstrated that at constant gold concentration and varying particle size, the best sensitivity was obtained when using larger particles of 63 nm. This trend was explained in terms of a higher target-to-particles ratio, as compared to smaller AuNPs. Using 63 nm particles we could differentiate the match from the mismatch sequences at concentrations down to 10 pM. Particle size was also found to affect the selectivity of the assay. Larger particles are more selective at lower target concentrations, but less selective at larger target concentrations, which is due to the lower surface curvature increasing the probability of multiple binding events. The results of our study show that colloidal biosensors based on AuNPs aggregation have an intrinsic limitation, related to the number of target molecules per particle.

ASSOCIATED CONTENT

Supporting Information Available: The following file is available free of charge: SNP_NPs-SI. The sensitivity limit of nanoparticle biosensors in the discrimination of single-nucleotide polymorphism. UV-Vis spectra during the hybridization process. UV-Vis spectra for different particle sizes at constant concentration. UV-Vis spectra and aggregation degree of 63 nm-particles at different concentrations. Table showing the ratio of target molecules per NP. Dynamic light scattering data. Hybridization process after thermal treatment. Hybridization degree for 63 nm-particles for different target concentrations.

AUTHOR INFORMATION

Corresponding Author

* **Marek Grzelczak, mgrzelczak@cicbiomagune.es**

ACKNOWLEDGMENT

This work was supported by the Spanish Ministerio de Economía y Competitividad MINECO (grants: MAT2013-46101-R, MAT2013-49375-EXP).

REFERENCES

(1) Antoniou, A. C.; Casadei, S.; Heikkinen, T.; Barrowdale, D.; Pylkäs, K.; Roberts, J.; Lee, A.; Subramanian, D.; De Leeneer, K.; Fostira, F.; *et al.* Breast-Cancer Risk in Families with Mutations in PALB2. *N. Engl. J. Med.* **2014**, *371*, 497–506.

(2) Figl, A.; Scherer, D.; Nagore, E.; Bermejo, J. L.; Dickes, E.; Thirumaran, R. K.; Gast, A.; Hemminki, K.; Kumar, R.; Schadendorf, D. Single Nucleotide Polymorphisms in DNA Repair Genes XRCC1 and APEX1 in Progression and Survival of Primary Cutaneous Melanoma Patients. *Mutat. Res. Mol. Mech. Mutagen.* **2009**, *661*, 78–84.

(3) Oliveira-Cunha, M.; Hadfield, K. D.; Siriwardena, A. K.; Newman, W. EGFR and KRAS Mutational Analysis and Their Correlation to Survival in Pancreatic and Periampullary Cancer: *Pancreas* **2012**, *41*, 428–434.

(4) Stenina, O. I.; Byzova, T. V.; Adams, J. C.; McCarthy, J. J.; Topol, E. J.; Plow, E. F. Coronary Artery Disease and the Thrombospondin Single Nucleotide Polymorphisms. *Int. J. Biochem. Cell Biol.* **2004**, *36*, 1013–1030.

(5) Monot, M.; Honoré, N.; Garnier, T.; Araoz, R.; Coppée, J.-Y.; Lacroix, C.; Sow, S.; Spencer, J. S.; Truman, R. W.; Williams, D. L.; *et al.* On the Origin of Leprosy. *Science* **2005**, *308*, 1040–1042.

(6) Suh, Y.; Vijg, J. SNP Discovery in Associating Genetic Variation with Human Disease Phenotypes. *Mutat. Res. Mol. Mech. Mutagen.* **2005**, *573*, 41–53.
(7) Ney, J. T.; Froehner, S.; Roesler, A.; Buettner, R.; Merkelbach-Bruse, S. High-Resolution Melting Analysis as a Sensitive Prescreening Diagnostic Tool to Detect KRAS, BRAF, PIK3CA, and AKT1 Mutations in Formalin-Fixed, Paraffin-Embedded Tissues. *Arch. Pathol. Lab. Med.* **2012**, *136*, 983–992.
(8) Malapelle, U.; Carlomagno, C.; Salatiello, M.; De Stefano, A.; De Luca, C.; Bianco, R.; Marciano, R.; Cimminiello, C.; Bellevicine, C.; De Placido, S.; *et al.* KRAS Mutation Detection by High-Resolution Melting Analysis Significantly Predicts Clinical Benefit of Cetuximab in Metastatic Colorectal Cancer. *Br. J. Cancer* **2012**, *107*, 626–631.
(9) Sorgenfrei, S.; Chiu, C.; Jr, R. L. G.; Yu, Y.-J.; Kim, P.; Nuckolls, C.; Shepard, K. L. Label-Free Single-Molecule Detection of DNA-Hybridization Kinetics with a Carbon Nanotube Field-Effect Transistor. *Nat. Nanotechnol.* **2011**, *6*, 126–132.
(10) Cisse, I. I.; Kim, H.; Ha, T. A Rule of Seven in Watson-Crick Base Pairing of Mismatched Sequences. *Nat. Struct. Mol. Biol.* **2012**, *19*, 623–627.
(11) Song, S.; Liang, Z.; Zhang, J.; Wang, L.; Li, G.; Fan, C. Gold-Nanoparticle-Based Multicolor Nanobeacons for Sequence-Specific DNA Analysis. *Angew. Chem. Int. Ed.* **2009**, *48*, 8670–8674.
(12) Huang, J.; Wu, Y.; Chen, Y.; Zhu, Z.; Yang, X.; Yang, C. J.; Wang, K.; Tan, W. Pyrene-Excimer Probes Based on the Hybridization Chain Reaction for the Detection of Nucleic Acids in Complex Biological Fluids. *Angew. Chem. Int. Ed.* **2011**, *50*, 401–404.
(13) Graham, D.; Mallinder, B. J.; Whitcombe, D.; Watson, N. D.; Smith, W. E. Simple Multiplex Genotyping by Surface-Enhanced Resonance Raman Scattering. *Anal. Chem.* **2002**, *74*, 1069–1074.
(14) Millis, M. P. Medium-Throughput SNP Genotyping Using Mass Spectrometry: Multiplex SNP Genotyping Using the iPLEX® Gold Assay. *Methods Mol. Biol. Clifton NJ* **2011**, *700*, 61–76.
(15) Patolsky, F.; Lichtenstein, A.; Willner, I. Detection of Single-Base DNA Mutations by Enzyme-Amplified Electronic Transduction. *Nat. Biotechnol.* **2001**, *19*, 253–257.
(16) Tahira, T.; Kukita, Y.; Higasa, K.; Okazaki, Y.; Yoshinaga, A.; Hayashi, K. Estimation of SNP Allele Frequencies by SSCP Analysis of Pooled DNA. *Methods Mol. Biol. Clifton NJ* **2009**, *578*, 193–207.
(17) Song, Y.; Zhang, W.; An, Y.; Cui, L.; Yu, C.; Zhu, Z.; Yang, C. J. Label-Free Visual Detection of Nucleic Acids in Biological Samples with Single-Base Mismatch Detection Capability. *Chem. Commun.* **2011**, *48*, 576–578.
(18) Elghanian, R.; Storhoff, J. J.; Mucic, R. C.; Letsinger, R. L.; Mirkin, C. A. Selective Colorimetric Detection of Polynucleotides Based on the Distance-Dependent Optical Properties of Gold Nanoparticles. *Science* **1997**, *277*, 1078–1081.
(19) Storhoff, J. J.; Elghanian, R.; Mucic, R. C.; Mirkin, C. A.; Letsinger, R. L. One-Pot Colorimetric Differentiation of Polynucleotides with Single Base Imperfections Using Gold Nanoparticle Probes. *J. Am. Chem. Soc.* **1998**, *120*, 1959–1964.
(20) Quan, K.; Huang, J.; Yang, X.; Yang, Y.; Ying, L.; Wang, H.; Wang, K. An Enzyme-Free and Amplified Colorimetric Detection Strategy: Assembly of Gold Nanoparticles through Target-Catalytic Circuits. *Analyst* **2015**, *140*, 1004–1007.
(21) Ma, C.; Wang, W.; Mulchandani, A.; Shi, C. A Simple Colorimetric DNA Detection by Target-Induced Hybridization Chain Reaction for Isothermal Signal Amplification. *Anal. Biochem.* **2014**, *457*, 19–23.
(22) Wang, Q.; Li, R.-D.; Yin, B.-C.; Ye, B.-C. Colorimetric Detection of Sequence-Specific microRNA Based on Duplex-Specific Nuclease-Assisted Nanoparticle Amplification. *Analyst* **2015**, *140*, 6306–6312.
(23) Turkevich, J.; Stevenson, P. C.; Hillier, J. A Study of the Nucleation and Growth Processes in the Synthesis of Colloidal Gold. *Discuss. Faraday Soc.* **1951**, *11*, 55–75.
(24) Jain, P. K.; Lee, K. S.; El-Sayed, I. H.; El-Sayed, M. A. Calculated Absorption and Scattering Properties of Gold Nanoparticles of Different Size, Shape, and Composition: Applications in Biological Imaging and Biomedicine. *J. Phys. Chem. B* **2006**, *110*, 7238–7248.
(25) Hurst, S. J.; Hill, H. D.; Mirkin, C. A. "Three-Dimensional Hybridization" with Polyvalent DNA−Gold Nanoparticle Conjugates. *J. Am. Chem. Soc.* **2008**, *130*, 12192–12200.
(26) Rasheed, P. A.; Sandhyarani, N. A Highly Sensitive DNA Sensor for Attomolar Detection of the BRCA1 Gene: Signal Amplification with Gold Nanoparticle Clusters. *Analyst* **2015**, *140*, 2713–2718.
(27) Yang, Y.; Li, C.; Yin, L.; Liu, M.; Wang, Z.; Shu, Y.; Li, G. Enhanced Charge Transfer by Gold Nanoparticle at DNA Modified Electrode and Its Application to Label-Free DNA Detection. *ACS Appl. Mater. Interfaces* **2014**, *6*, 7579–7584.
(28) Xu, H.; Wang, L.; Ye, H.; Yu, L.; Zhu, X.; Lin, Z.; Wu, G.; Li, X.; Liu, X.; Chen, G. An Ultrasensitive Electrochemical Impedance Sensor for a Special BRCA1 Breast Cancer Gene Sequence Based on Lambda Exonuclease Assisted Target Recycling Amplification. *Chem. Commun.* **2012**, *48*, 6390–6392.
(29) Bastús, N. G.; Comenge, J.; Puntes, V. Kinetically Controlled Seeded Growth Synthesis of Citrate-Stabilized Gold Nanoparticles of up to 200 Nm: Size Focusing versus Ostwald Ripening. *Langmuir* **2011**, *27*, 11098–11105.
(30) Hurst, S. J.; Lytton-Jean, A. K. R.; Mirkin, C. A. Maximizing DNA Loading on a Range of Gold Nanoparticle Sizes. *Anal. Chem.* **2006**, *78*, 8313–8318.
(31) Enustun, B. V.; Turkevich, J. Coagulation of Colloidal Gold. *J. Am. Chem. Soc.* **1963**, *85*, 3317–3328.
(32) Naiser, T.; Ehler, O.; Kayser, J.; Mai, T.; Michel, W.; Ott, A. Impact of Point-Mutations on the Hybridization Affinity of Surface-Bound DNA/DNA and RNA/DNA Oligonucleotide-Duplexes: Comparison of Single Base Mismatches and Base Bulges. *BMC Biotechnol.* **2008**, *8*, 48.
(33) Reynolds, R. A.; Mirkin, C. A.; Letsinger, R. L. Homogeneous, Nanoparticle-Based Quantitative Colorimetric Detection of Oligonucleotides. *J. Am. Chem. Soc.* **2000**, *122*, 3795–3796.
(34) Murphy, C. J.; Gole, A. M.; Stone, J. W.; Sisco, P. N.; Alkilany, A. M.; Goldsmith, E. C.; Baxter, S. C. Gold Nanoparticles in Biology: Beyond Toxicity to Cellular Imaging. *Acc. Chem. Res.* **2008**, *41*, 1721–1730.
(35) Ghosh, S. K.; Pal, T. Interparticle Coupling Effect on the Surface Plasmon Resonance of Gold Nanoparticles: From Theory to Applications. *Chem. Rev.* **2007**, *107*, 4797–4862.
(36) Liu, Y.; Liu, Y.; Mernaugh, R. L.; Zeng, X. Single Chain Fragment Variable Recombinant Antibody Functionalized Gold Nanoparticles for a Highly Sensitive Colorimetric Immunoassay. *Biosens. Bioelectron.* **2009**, *24*, 2853–2857.
(37) D'Abramo, M.; Castellazzi, C. L.; Orozco, M.; Amadei, A. On the Nature of DNA Hyperchromic Effect. *J. Phys. Chem. B* **2013**, *117*, 8697–8704.

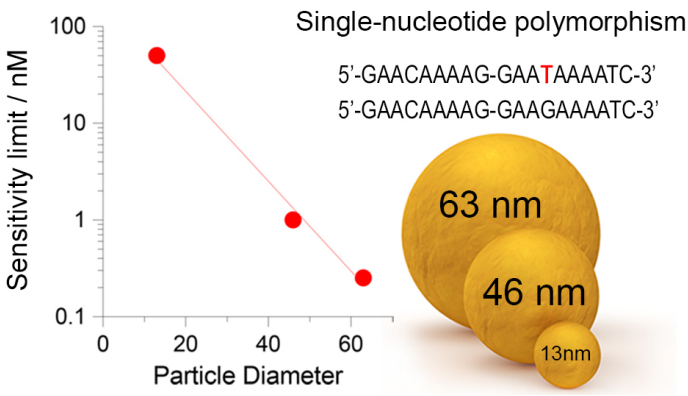
Single-nucleotide polymorphism
5'-GAACAAAAG-GAATAAAATC-3'
5'-GAACAAAAG-GAAGAAAATC-3'
Sensitivity limit / nM
100
10
1
0.1
0
20
40
60
Particle Diameter
63 nm
46 nm
13nm

for TOC only